Title

Type I interferon responses contribute to immune protection against mycobacterial infection

Authors

Andrea Szydlo-Shein[1], Blanca Sanz-Magallón Duque de Estrada[1], Joshua Rosenheim[1], Carolin T. Turner[1], Evdokia Tsaliki[1], Marc C. I. Lipman[2,3], Heinke Kunst[4,5], Gabriele Pollara[1], Philip M. Elks[6], Jean-Pierre Levraud[7], Elspeth M. Payne[8], Mahdad Noursadeghi[1], Gillian S. Tomlinson[1]*

Affiliations

[1]Division of Infection and Immunity, University College London, London, UK

[2]Respiratory Medicine, Royal Free London NHS Foundation Trust, London, UK

[3]UCL Respiratory, University College London, London, UK

[4]Barts Health NHS Trust, London, UK

[5]Blizard Institute, Queen Mary University of London, London, UK

[6]The Bateson Centre, School of Medicine and Population Health, The University of Sheffield, Sheffield, UK

[7]Université Paris-Saclay, CNRS UMR9197, Institut Pasteur, Université Paris-Cité, Institut des Neurosciences Paris-Saclay, 91400 Saclay, France

[8]Research Department of Haematology, Cancer Institute, University College London, London, UK

*Corresponding author

Corresponding author

Gillian S. Tomlinson, Email: g.tomlinson@ucl.ac.uk

ABSTRACT

Reasons for the spectrum of severity of active tuberculosis (TB) disease are incompletely understood. We sought to identify master regulators of host immune responses that determine disease severity in pulmonary TB. We performed molecular profiling of human in vivo immune responses to discover associations with the extent of radiographic TB disease in a patient cohort. We then undertook mechanistic studies to test causality for the observed associations using the zebrafish larval *Mycobacterium marinum* infection model. Transcriptional profiling of human immune recall responses to tuberculin skin test (TST) challenge, a surrogate for immune responses to TB in the lung, revealed that type I interferon activity in the TST transcriptome was inversely associated with radiological disease severity. Abrogation of type I interferon signalling, achieved by CRISPR-mediated mutagenesis of *stat2*, led to increased susceptibility of zebrafish larvae to *M. marinum* infection, as a result of reduced recruitment of myeloid cells required to restrict mycobacterial growth, to the site of disease. Our data support a host protective role for type I interferon responses in mycobacterial infection, with potential applications for risk-stratification of adverse outcomes and development of a host-directed therapy to mitigate against severe disease.

ONE SENTENCE SUMMARY

Type I interferon responses contribute to host immune protection in mycobacterial infection by recruitment of myeloid cells to the site of disease.

INTRODUCTION

Mycobacterium tuberculosis (Mtb) infection results in diverse clinical manifestations, ranging from asymptomatic infection to active tuberculosis (TB), which comprises an enormous spectrum of disease severity *(1, 2)*. Although we know that immune responses contribute to the risk of disease, current understanding of the role of immune response variation in disease severity is limited. Identification of immune correlates of disease severity may offer new insights into the immune pathways that contribute to protection and pathogenesis. This is necessary to enable novel vaccine design and evaluation, stratify disease risk in people who become infected and inform development of novel host-directed therapies to shorten treatment regimens, mitigate against antimicrobial resistance, and against the chronic sequelae of tissue injury in TB *(3)*.

Variation in tissue immunology of human TB at the site of established disease is likely confounded by differences in the chronicity of the disease process. To overcome this limitation, we evaluated in vivo immune responses at the site of a standardised antigenic challenge using the tuberculin skin test (TST). We have previously shown that transcriptional profiling of skin biopsies from the site of the TST provides comprehensive molecular and systems level evaluation of human in vivo immune responses to Mtb with significantly greater sensitivity than conventional clinical and histological assessments *(4, 5)*. The TST gene signature is enriched within pulmonary TB granulomas and accounts for genome-wide differences in the transcriptomes of TB infected lung compared to healthy lung tissue *(5, 6)*. Therefore, the TST provides a faithful and readily accessible surrogate to study immune responses at the site of TB disease.

In the present study, we identified quantitative variation in immune pathways in the TST response correlated with the severity of human TB disease, and then tested the hypothesis that these pathways were causally related to outcomes of *Mycobacterium marinum* infection in zebrafish larvae. This natural host-pathogen interaction generates granulomatous inflammation that recapitulates key aspects of human TB pathology and in particular, provides unparalleled opportunities to study innate immune responses in isolation, given the absence of functional adaptive immunity until 3-4 weeks *(7)*. Our innovative strategy revealed an inverse relationship between type I interferon activity and radiographic severity of human TB, suggesting a host-protective role for type I interferons, that we confirmed in zebrafish larvae by showing that mutagenesis of *stat2* to model abrogation of downstream type I interferon signalling led to increased severity of *M. marinum* infection.

RESULTS

Outlier analysis of the TST transcriptome defines human in vivo immune responses to active tuberculosis

We supplemented data from our previously reported TST transcriptional responses *(8)* to provide a total sample size of 51 people with microbiologically confirmed pulmonary TB who were within one month of commencing anti-tuberculous chemotherapy (Table 1, Fig. S1A, B). We evaluated disease severity using a published radiographic scoring system which incorporates extent of disease and the presence of cavitation on chest x-ray *(9)*. In order to capture the inter-individual variation in immune response to the mycobacterial challenge, outlier profile analysis *(10)* was used to identify transcripts in the TST of each individual that were significantly enriched compared to gene expression in control data from skin biopsies at the site of saline injections. The integrated list of outlier genes statistically enriched in TST samples compared to control saline samples from all 51 individuals defined an active TB TST transcriptome comprised of 3222 transcripts. This analysis revealed that although some aspects of the TST response are consistent in all people, there is also considerable variability between individuals (Fig. S1C). The 3222 transcripts identified by this approach, were enriched for canonical pathways involved in cell mediated responses, consistent with our previous description of the TST gene signature identified by conventional differential gene expression analysis *(5, 8)* (Fig. S1D).

Reduced type I interferon activity in the TST transcriptome is associated with increased severity of human TB disease

Next, we sought to identify immunological pathways correlated with disease severity. We identified individual genes in the TST transcriptome that showed statistically significant correlations with the

radiographic severity score. We subjected these genes to Ingenuity Pathway Analysis upstream regulator analysis to collate groups of co-regulated genes (Fig. 1A and Fig. S2A). These were annotated by their upstream regulators at the level of cytokines, transmembrane receptors, kinases and transcriptional regulators, representing the key components of signalling pathways which mediate immune responses. To provide increased confidence that these modules represented co-regulated genes in each molecular pathway, we retained only those that had significantly greater co-correlated expression than modules of genes randomly selected from our TST transcriptomes *(11)*. 111 modules were identified among genes inversely correlated with radiographic TB severity, suggesting they may contribute to host protection against severe disease (Fig. 1A-C and Fig. S2B). These included transcriptional modules representing pro-inflammatory cytokine activity (tumour necrosis factor alpha and interleukin (IL)1 beta), interferon gamma and T cell activity, consistent with existing evidence predominantly supporting their protective roles in TB *(12)* (Fig. 1B). In addition, we found enrichment of multiple co-regulated gene networks attributed to type I interferon signalling, suggesting that type I interferon responses may also contribute to host protection in mycobacterial infection (Fig. 1B, C). Interferon gamma was also predicted to regulate one of only two small putative networks within genes positively correlated with disease severity; the other driven by TCL1A, an AKT kinase activator that promotes cellular survival *(13)* (Fig. S2C).

To validate the immunological responses predicted to be associated with disease severity by upstream regulator analysis, we quantified the expression of two independently derived and largely non-overlapping type I interferon inducible gene modules reflecting the biological activity of type I interferons (Table S1) *(5, 8)*, within the TB TST transcriptome (Fig. 1D). This provided independent validation of the inverse relationship between type I interferon responses and radiographic severity of TB (Fig. 1E), suggestive of a host-protective role. By contrast, the expression of the entire TST transcriptome and that of three distinct independently derived interferon gamma inducible gene modules *(5)* (Table S1) did not correlate with disease severity (Fig. S3).

stat2 CRISPant zebrafish larvae exhibit increased susceptibility to *M. marinum* infection

The TST transcriptome does not solely reflect anti-mycobacterial T cell memory *(4)* and type I interferons are primarily induced following activation of innate immune recognition pathways *(14)*. Therefore, to evaluate whether impaired type I interferon responses cause more severe mycobacterial disease, we exploited the zebrafish larval *M. marinum* infection model, which allows exclusive assessment of innate immunity *(7)*. The mammalian canonical type I interferon signalling pathway is highly conserved in zebrafish *(15, 16)* (Fig. 2A). First, we confirmed that intravenous *M. marinum* infection of wild type zebrafish larvae induces a type I interferon response, as evidenced by enrichment for two distinct independently derived transcriptional modules reflecting type I interferon activity *(11, 16)* (Table S1) within genome-wide transcriptomic data obtained after four days of mycobacterial growth (Fig. 2B, C). To block downstream type I interferon signalling we used CRISPR-mediated mutagenesis of *stat2*, a subunit of the interferon stimulated gene factor (ISGF)3, the principal transcription factor complex which induces expression of type I interferon stimulated genes (ISG) *(17–19)*, for which there is a single zebrafish orthologue *(15)* (Fig. 2A). Injection of three guide RNA/Cas9 ribonucleoprotein (RNP) complexes each targeting a distinct *stat2* exon, into one cell stage wild type zebrafish embryos led to >90% efficient mutagenesis, confirmed by next-generation sequencing (Fig. S4A and Fig. S5A). We verified loss of functional downstream type I interferon signalling by showing that induction of the classical ISG Mxa *(16, 19)* by recombinant interferon phi 1, measured by expression of a reporter *mxa:mCherry* transgene, was significantly attenuated in *stat2* CRISPants compared to siblings injected with “scrambled” (negative control) RNPs designed to lack genomic targets (Fig. S4B and Fig. S5B-C). *stat2* CRISPants developed normally up to five days post-fertilisation (Fig. S5B).

There was no difference in survival of *M. marinum* infected *stat2* CRISPants and scrambled RNP injected siblings (Fig. 3A, B) within the timeframe of our experiments. However, mycobacterial burden, the number of bacterial foci and the spatial dissemination of bacteria, determined by quantitation of fluorescent foci of *M. marinum*, were all significantly higher in intravenously infected *stat2* CRISPants compared to control RNP injected siblings, indicative of more severe disease (Fig. 3A, C-E). These findings are consistent with a host protective role for type I interferons in mycobacterial infection, as suggested by our observation of an association between reduced type I interferon activity and increased disease severity in human TB (Fig. 1).

148 **Steady state neutrophil numbers are reduced in *stat2* CRISPant zebrafish larvae**

149 Macrophages are critically important for control of *M. marinum* infection in zebrafish larvae *(20–22)*
150 and neutrophils may also contribute to mycobacterial killing *(23, 24)*. Therefore, to investigate the
151 mechanisms by which *stat2* deficiency leads to worse mycobacterial infection we used transgenic
152 zebrafish lines with fluorescent immune cell lineages to generate *stat2* CRISPants that have
153 fluorescent macrophages or neutrophils. First, we asked whether *stat2* disruption impacted steady
154 state macrophage or neutrophil numbers. We demonstrated by quantitative fluorescence
155 microscopy, using integrated fluorescence as a surrogate for cell number, that *stat2* deficiency did
156 not affect baseline macrophage numbers (Fig. 4A, B). However, it was associated with reduced
157 neutrophil numbers (Fig. 4C, D).

158 **Recruitment of macrophages but not neutrophils to the site of sterile injury is *stat2***
159 **dependent**

160 Type I interferons have previously been shown to influence cellular migration *(14, 25)*. Therefore,
161 we tested macrophage and neutrophil recruitment in *stat2* CRISPants using a tailfin transection
162 model of sterile injury, most commonly used to evaluate neutrophil recruitment *(26)* (Fig. S4C). The
163 timing of neutrophil homing to the site of sterile tail fin transection was normal in *stat2* CRISPants,
164 with maximal accumulation at six hours and dissipation of recruited cells becoming evident by 24
165 hours, similar to that of control RNP injected embryos (Fig. 5A, B) and in keeping with previous
166 studies *(26, 27)*. Despite baseline neutropenia, the number of neutrophils at the wound site at the
167 point of maximal recruitment in *stat2* CRISPants exceeded that of control RNP injected embryos.
168 But by 24 hours the number of neutrophils at the injury site was significantly reduced in *stat2*
169 CRISPants, likely reflecting the attenuated increase in total neutrophil numbers in response to the
170 acute inflammatory challenge (Fig. 5C, D).

171 As previously reported, macrophage recruitment to the tail wound site was slower than that of
172 neutrophils *(27, 28)*. Very few macrophages were present at the tailfin transection site by one hour
173 in either *stat2* disrupted or control transgenic larvae, but recruitment progressively increased until 24
174 hours in both groups (Fig. 6). Fewer macrophages were found in the vicinity of the wound site at all
175 time points post-injury in *stat2* CRISPant transgenic embryos compared to control RNP injected
176 siblings, the majority being located outwith the tailfin (Fig. 6). Taken together these data suggest that
177 *stat2* is necessary for macrophage recruitment but non-essential for neutrophil recruitment to a
178 sterile injury site. In addition, baseline neutropenia did not impact the number of cells localised to the
179 wound at peak neutrophil recruitment.

180 **Recruitment of myeloid cells to the site of *M. marinum* infection is *stat2* dependent**

181 Next we focused on macrophage recruitment to the site of mycobacterial infection because this has
182 been reported to be crucial for control of *M. marinum* growth in zebrafish larvae *(21)*. We found a
183 significant reduction in the number of macrophages recruited to the site of localised hindbrain
184 *M. marinum* infection in *stat2* deficient transgenic zebrafish larvae compared to their counterparts
185 injected with scrambled RNPs (Fig. S4D and Fig. 7A, B). We then evaluated whether *stat2* disruption
186 affected recruitment of neutrophils to the site of mycobacterial infection. We found that in contrast to
187 their normal peak recruitment to a sterile wound, the number of neutrophils attracted to the site of
188 mycobacterial disease was also significantly diminished in *stat2* CRISPants (Fig 7C, D). Collectively,
189 these results demonstrate that myeloid cell recruitment to the site of *M. marinum* infection is *stat2*
190 dependent.

191 In total, the recruitment studies suggest that *stat2* disruption leads to a broad defect in macrophage
192 recruitment to both infectious and non-infectious inflammatory foci. By contrast, *stat2* is non-essential
193 for neutrophil migration to sterile injury. The latter finding is consistent with defective migration, rather
194 than neutropenia, being the principal mechanism for reduced neutrophil numbers at the site of
195 *M. marinum* infection.

196 **DISCUSSION**

197 We have taken an innovative approach, combining molecular and systems level evaluation of human
198 immune responses to a standardised experimental challenge, to identify master regulators of

biological pathways associated with TB disease severity. We experimentally validated host factors responsible for differences in phenotype using a relevant, tractable animal model which represents a natural host-pathogen pairing *(7)*. Molecular interrogation of human in vivo responses to Mtb revealed that reduced type I interferon activity within the TST transcriptome was associated with worse pulmonary disease. Deficient type I interferon signalling, achieved by genetic disruption of *stat2*, led to more severe mycobacterial infection in zebrafish larvae, via a mechanism involving impaired recruitment of macrophages and neutrophils to the site of disease and reduced neutrophil numbers at baseline. Taken together our results demonstrate an important role for type I interferon responses in contributing to innate immune protection against mycobacterial disease.

Peripheral blood interferon-inducible gene expression that diminishes with successful treatment is detectable in human active TB *(29–31)*. These transcriptional signatures comprise both type I and type II interferon inducible genes but have mainly been interpreted as type I interferon responses, fostering the view that type I interferons are detrimental to the host in human TB. Mouse data predominantly suggest that type I interferon responses contribute to increased susceptibility to mycobacterial infection by mechanisms including antagonism of IL1 mediated protection *(32–34)* and reduced responsiveness of macrophages to interferon gamma *(35)*. However, this phenotype has not been universally observed, likely due to differences in host and pathogen genetics *(36)*. Moreover, impaired type I interferon responses are generally associated with relatively minor differences in bacterial burden or survival *(36)*. Of note, Mtb is not a natural mouse pathogen, and this approach may not model host-pathogen interactions in human TB faithfully *(37)*.

In support of a protective role for type I interferons, adjunctive interferon alpha therapy in addition to conventional anti-tuberculous antibiotic treatment led to symptomatic and radiological improvement, with a reduction in bacterial burden in respiratory tract samples, in small-scale human studies *(38–40)*. In keeping with this, an early peripheral blood type I interferon-inducible gene signature predicts successful BCG-induced protection of macaques from subsequent Mtb challenge *(41)*. Type I interferon mediated restriction of mycobacterial growth in in vitro granulomas comprising collagen impregnated microspheres containing Mtb infected human peripheral blood mononuclear cells (PBMC) *(42)* also suggests that type I interferon responses benefit the host.

Our observation of reduced recruitment of macrophages to the site of disease is likely the most important factor driving increased susceptibility to *M. marinum* infection in *stat2* CRISPants. Although macrophages have been implicated in the dissemination of *M. marinum* in zebrafish larvae *(20, 43)*, reduction of total macrophage numbers, impaired macrophage migration to the site of mycobacterial infection or failure to control intracellular bacterial growth within macrophages have all been associated with poor outcome *(20–22, 44, 45)*. In contrast, increasing macrophage numbers via augmentation of M-CSF signalling either pre- or post-granuloma formation, promotes resistance to *M. marinum* infection by reducing granuloma necrosis, with consequent curtailment of extracellular mycobacterial growth *(21)*. The recent report that human genetically inherited CCR2 deficiency is associated with reduced pulmonary recruitment of monocytes, resulting in depleted numbers of functionally normal alveolar macrophages and increased susceptibility to mycobacteria, is also consistent with the notion that adequate numbers of macrophages are important for protective anti-mycobacterial immunity *(46)*.

The reduction in neutrophils present at the site of *M. marinum* infection in *stat2* CRISPants may have arisen due to baseline neutropenia, defective migration or both combined. On the basis that steady state neutropenia did not affect the timing and magnitude of peak neutrophil recruitment to sterile injury, impaired migration is probably the main driver of this phenotype, which likely also contributed to increased severity of mycobacterial disease. Previous data show that reduced access of neutrophils to mycobacteria leads to increased bacterial burden in a zebrafish line in which neutrophils express mutant *cxcr4*, resulting in peripheral neutropenia and impaired neutrophil recruitment to sites of inflammation, due to their retention in haematopoietic tissue *(23, 47)*.

Our study has some limitations. We were not able to address the reasons for variation in type I interferon activity in our human cohort. Serum samples for measurement of autoantibodies to type I interferons are not available and our sample size is insufficient for robust detection of associations between genetic variation and the expression levels of type I interferon signalling pathway genes. We were also unable to completely disentangle whether reduced neutrophil recruitment to the site of *M. marinum* infection was a consequence of neutropenia or impaired migration. We have not

determined the mechanism by which attenuated type I interferon signalling leads to reduced myeloid cell recruitment to *M. marinum*. The expression of several chemokines is type I interferon inducible *(25, 48, 49)* and the CCR2-CCL2 and CXCR3-CXCL11 chemokine axes are known to be involved in macrophage recruitment to *M. marinum (43, 50)*. Future studies are required to test the hypothesis that *stat2* mutagenesis disrupts chemokine-mediated cellular recruitment to the site of mycobacterial disease. Nonetheless, our work provides new insights into type I interferon mediated host protection against mycobacterial infection.

Variation in type I interferon responses may arise due to genetically or epigenetically encoded variation in the immune response to Mtb, neutralising type I interferon auto-antibodies, burden and virulence of the mycobacterial inoculum and stochasticity in the immune response pathway following exposure *(51–55)*. A central tenet of all these possibilities is that differences in the host immune response to Mtb lead to differences in disease severity. Our findings have potential implications for risk stratification of individuals in whom any of these mechanisms predisposing to low type I interferon activity are identified. In active TB, such individuals could be targeted for longer or more intensive drug regimens, or adjunctive type I interferon therapy delivered to the respiratory tract, to mitigate against severe disease. Early intervention with type I interferon treatment, before destruction of the lung parenchyma, is likely to be crucial to augment macrophage containment of Mtb, but timing and duration of therapy will require evaluation in relatively large-scale experimental medicine trials.

MATERIALS AND METHODS

Ethics statement

The study was approved by the London Bloomsbury Research Ethics Committee (16/LO/0776). Written informed consent was obtained from all participants.

Study design

We aimed to identify master regulators of human immune responses that correlate with severity of TB disease, using transcriptional profiling of biopsies from the TST as a surrogate for immune responses to TB in the lung and to test causation for observed associations by genetic manipulation of identified upstream regulator molecules in the zebrafish larval mycobacterial infection model. To encompass a broad spectrum of disease severity we recruited 51 adults (>18 years) from four London hospitals, newly diagnosed with smear or culture positive pulmonary TB, who were within four weeks of starting treatment. This is in keeping with the median sample size of previous studies which have successfully demonstrated a relationship between severity of TB disease and immunological parameters *(29, 56–59)*. Individuals with coincident human immunodeficiency virus infection, malignancy, taking immunomodulatory therapy, a history of immunization within the preceding two weeks or previous keloid formation, or unable to give informed consent were excluded. Study participants underwent intradermal injection of 0.1 ml of two units of tuberculin (AJ Vaccines) or saline in the volar aspect of the forearm as previously described *(4, 5, 8)*. At 48 hours clinical induration at the injection site was measured, immediately prior to sampling by 3mm punch biopsy as previously described *(4, 5)*. Additional saline samples from individuals with cured or latent TB, BCG vaccine recipients and healthy volunteers have been described previously *(8)*.

RNA purification from skin biopsy and zebrafish embryo samples

Skin biopsies were homogenized as previously described *(8)*. Pooled zebrafish embryos (25-30 per experimental condition) collected in Qiazol (Qiagen) were homogenized in CK14 lysing kit tubes (Bertin Instruments) using a Precellys Evolution homogenizer (Bertin Instruments) for 10-20 seconds at 5500 rpm. Total RNA from skin biopsies and zebrafish samples was purified using the RNEasy mini and micro kits (Qiagen), respectively, according to the manufacturer's instructions. Genomic DNA was removed using the TURBO DNA-free kit (ThermoFisher).

Transcriptional profiling of skin biopsy and zebrafish larval samples

Genome-wide mRNA sequencing was performed as previously described *(8, 60)*. Complementary DNA (cDNA) libraries were prepared using the KAPA HyperPrep kit (Roche). Sequencing was performed in paired-end mode with the NextSeq 500 High Output 75 Cycle Kit (Illumina) using the NextSeq500 system (Illumina) according to the manufacturer's instructions, generating a median of 22 million (range 12.3-27.9 million) 41 base pair reads per human sample and 16.8 million (range

306 15.1-18.1 million) reads per zebrafish sample. Transcript alignment and quantitation against the
307 Ensembl GRCh38 human genome assembly release 100 or GRCz11 zebrafish genome assembly
308 release 104 was performed using Kallisto *(61)*. Transcript-level output counts and transcripts per
309 million (TPM) values were summed on gene level and annotated with Ensembl gene ID, gene name,
310 and gene biotype using the R/Bioconductor packages tximport and BiomaRt *(62, 63)*. Downstream
311 analysis was performed using R 3.6.3 on log2 transformed TPM values for protein-coding genes
312 only. TPM values <0.001 were set to 0.001 prior to log2 transformation. To determine the need for
313 and effect of batch correction in the human data, principal component analysis (PCA) was performed
314 using the prcomp R function on the integrated list of 6802 genes with the 10% lowest variance in
315 expression for each library preparation date. This revealed separation of three samples in PC1, likely
316 accounted for by lower RNA concentrations or RIN values compared to the rest of the dataset (Fig.
317 S1A). After batch correction performed using the ComBat function of the sva R package *(64)*,
318 allocating samples with PC1 score <0 and >0 to separate batches, this was no longer evident (Fig.
319 S1B).

320 **Radiographic quantitation of TB severity**

321 Disease severity was evaluated by estimating the extent of radiographic abnormalities and whether
322 cavitation was present on chest x-ray at the time of diagnosis, as previously described *(8, 9)*.

323 **Outlier analysis**

324 The BioBase Bioconductor R package was used to perform outlier analysis based on the z-score
325 outlier detection (ZODET) algorithm *(10)*, to identify transcripts in each TST sample whose
326 expression was significantly higher than the mean expression in control saline samples (>2SD,
327 p value <0.05), with a fold difference filter of >1 log2. Chi-squared tests implemented in R were then
328 used to identify outlier genes statistically enriched in TST samples compared to saline samples,
329 using a p value <0.05. To avoid type 2 error no correction for multiple testing was used in this
330 analysis. In instances where multiple Ensembl gene IDs were associated with a single gene symbol,
331 duplicate gene symbols were removed to retain the replicate with the highest expression for each
332 sample.

333 **Pathway enrichment analysis**

334 The biological pathways represented by the TST transcriptome were identified by Reactome
335 pathway enrichment analysis using XGR as previously described *(65, 66)*. For visualization, 15
336 pathway groups were identified by hierarchical clustering of Jaccard indices to quantify similarity
337 between the gene compositions of each pathway. For each group the pathway term with the largest
338 number of annotated genes was then selected as representative of enriched biology.

339 **Upstream regulator analysis**

340 TST transcriptome genes whose expression was significantly correlated with radiographic severity
341 of TB disease were identified by Spearman rank correlation, p value <0.05, without correction for
342 multiple testing, to prevent type 2 error. Genes positively and negatively correlated with disease
343 severity were separately subjected to Ingenuity Pathway Analysis (Qiagen) to identify upstream
344 molecules responsible for their transcriptional regulation. This analysis was restricted to molecules
345 annotated with the following functions: cytokine, transmembrane receptor, kinase and transcriptional
346 regulator, representing the canonical components of pathways which mediate transcriptional
347 reprogramming in immune responses. Enriched molecules with an adjusted p value <0.05 were
348 considered statistically significant.

349 **Upstream regulator functional modules**

350 TST gene modules representing the functional activity of their upstream molecule were identified as
351 previously described *(11)*. In brief, we calculated the average correlation coefficient for pairwise
352 correlations of the expression levels of the target genes associated with each predicted upstream
353 regulator. We compared these to the distribution of average correlation coefficients obtained from
354 100 iterations of randomly selecting equivalent sized groups of genes from the TST transcriptome.
355 Only target gene modules with average correlation coefficients higher than the mean of the
356 distribution of equivalent sized randomly selected groups by ≥2 SD (Z score ≥2) with false discovery
357 rate <0.05, were retained. We visualised these upstream regulator modules as network diagrams

using the Force Atlas two algorithm in Gephi v0.9.2 *(67)*, depicting all statistically over-represented molecules (false discovery rate <0.05) predicted to be upstream of ≥4 target genes.

Transcriptional modules

Interferon inducible transcriptional module gene lists are provided in Table S1. Independently derived human type I and type II interferon inducible gene modules were described previously *(5, 8, 11)*. Two further modules were derived to distinguish type I or type II interferon inducible gene expression using published transcriptional data for primary human keratinocytes stimulated with a selection of cytokines (Gene Expression Omnibus accession: GSE36287) *(68)*. Stimulus-specific modules for type I interferon (interferon alpha) and type II interferon (interferon gamma) were derived by selecting genes overexpressed >4-fold in the cognate cytokine condition relative to all non-cognate conditions combined (paired t test with α of $p<0.05$ without multiple testing correction), excluding genes also induced by each non-cognate cytokine condition, using the same criteria. The babelgene R package (https://igordot.github.io/babelgene/) was used to convert human gene symbols to their respective zebrafish orthologues to generate the zebrafish Stat1 module, excluding zebrafish genes reported to be an orthologue of more than one human gene. The zebrafish type I interferon inducible gene module comprises 360 genes whose expression was significantly induced (≥2 fold, adjusted p value <0.05) six hours after intravenous injection of three day post-fertilisation (dpf) larvae with 1 nl of recombinant interferon phi 1 protein (1 mg/ml) as previously described *(16)*.

Venn diagrams

Area-proportional Venn diagrams visualizing the overlap between constituent genes in transcriptional modules were generated using BioVenn *(69)*.

Zebrafish husbandry

Zebrafish were raised and maintained at 28.5°C following a 14/10 light/dark cycle according to standard protocols *(70)* in University College London (UCL) and Neuro-PSI Zebrafish Facilities. All work was approved by the British Home Office (Project License PP8780756) and the French Ministry for Research and Higher Education (Project Licence 39238). All experiments were performed in accordance with the relevant guidelines and regulations, on larvae up to five days post-fertilisation, before they are protected under the Animals (Scientific Procedures) Act. Adult zebrafish were spawned to collect embryos for experiments. Table S2 lists the lines used in this study *(26, 71, 72)*. Embryos were maintained at 28.5°C in egg water containing 60 µg/ml Tropic Marin Sea Salt (Norwood Aquarium) and anaesthetised with egg water containing 200 µg/ml buffered tricaine (3-aminobenzoic acid ethyl ester) (Sigma-Aldrich) during injection, tail fin transection and imaging. Larvae used for in vivo imaging were maintained in egg water supplemented at 24 hours post-fertilisation (hpf) with 0.003% PTU (1-phenyl-2-thiourea) (Sigma-Aldrich) to inhibit melanisation.

CRISPant Generation

To maximise the likelihood of loss of functional protein we employed a previously described triple-exon targeting approach *(73)*, with the modification that Cas9 protein was not diluted before use. CRISPR RNA (crRNA) (Alt-R CRISPR-Cas9 crRNA), tracrRNA (Alt-R CRISPR-Cas9 tracrRNA) and recombinant Cas9 protein (Alt-R Streptococcus pyogenes Cas9 Nuclease V3) were obtained from Integrated DNA Technologies (IDT). Three pre-designed crRNAs targeting distinct exons were selected for the *stat2* gene, prioritizing those that targeted early, asymmetric (not divisible by three) exons common to both protein-coding transcripts, with low off-target and high on-target scores and in a genomic position which allowed design of primers flanking the target site to generate a ~200 bp amplicon, for verification of mutagenesis by next generation sequencing (MiSeq). crRNA sequences and genomic locations are provided in Table S3. To generate gRNAs equal volumes of crRNA and tracrRNA diluted to 61 µM in Duplex buffer (IDT) were annealed at 95°C for 5 minutes. Equal volumes of gRNA (61 µM) and Cas9 protein (61 µM) were incubated at 37°C for 5 minutes to assemble separate 30.5 µM ribonucleoproteins (RNPs) for each target. Equal volumes of the three RNPs were pooled, prior to injection giving a final concentration of 10.2 µM for each. Negative control "scrambled" crRNAs computationally designed to be non-targeting (Alt-R CRISPRCas9 Negative Control crRNA #1, #2, #3) were prepared and pooled as described above. 0.5 nl of pooled *stat2* RNPs or scrambled RNPs was injected into the yolk sac of single-cell stage wild type or transgenic zebrafish embryos before cell inflation as previously described *(73)*. After injections embryos were

411 transferred into sterile petri dishes with fresh egg water and maintained at 28.5°C to the appropriate
412 age for experiments, as described below.

413 **Interferon phi 1 stimulation**

414 Three dpf *stat2* CRISPant *Tg(mxa:mCherry)* larvae and scrambled RNP injected siblings were
415 injected in the coelomic cavity with 1 nl of recombinant zebrafish interferon phi 1 protein (1.25 mg/ml),
416 produced as previously described *(74)*. *stat2* and control CRISPants were shuffled so that injections
417 were performed blindly. Bovine serum albumin (BSA) (1.25 mg/ml) was injected as a control.
418 Interferon phi 1 and BSA solutions were supplemented with 0.2% phenol red (Sigma-Aldrich) to
419 visualize the inoculum. Induction of Mxa reporter expression was determined by fluorescence
420 microscopy 24 hours post-injection.

421 ***M. marinum* infection**

422 *M. marinum* M strain expressing the pmsp12 mWasabi *(75)* or psMT3 mCherry plasmid *(76)* was
423 cultured using Middlebrook 7H10 agar (Becton Dickinson and Company) supplemented with 0.5%
424 oleic acid/albumin/dextrose/catalase (OADC) (Becton Dickinson and Company), 0.5% glycerol
425 (Sigma-Aldrich) and hygromycin (50 µg/ml) (Fisher Scientific). To generate bacterial suspensions for
426 injection, *M. marinum* from agar plates was cultured statically at 28.5°C for 24-36 hours in 10 ml
427 Middlebrook 7H9 broth (Becton Dickinson and Company) supplemented with 10%
428 albumin/dextrose/catalase (ADC) (Becton Dickinson and Company) and hygromycin (50 µg/ml)
429 (Fisher Scientific). Bacteria were harvested at mid-log growth (optical density (OD)600nm 0.7–1),
430 (OD)600nm 1 representing 10^8 colony forming units (cfu)/ml, washed three times in phosphate
431 buffered saline (PBS) (Gibco) and resuspended in 2% polyvinylpyrrolidone (PVP)40 (Sigma-
432 Aldrich)/PBS containing 10% phenol red (Sigma-Aldrich) to aid visualisation of injections *(77)*.

433 Zebrafish embryos were manually dechorionated using jeweller's forceps (Dumont #5, World
434 Precision Instruments) prior to bacterial infection. To generate systemic infection, 400 cfu
435 *M. marinum* in a volume of 1 nl were microinjected into the caudal vein of embryos staged at
436 28-30 hpf. Four days post-infection, embryos were either subjected to fluorescence microscopy to
437 measure disease severity or 25-30 per condition pooled and harvested in Qiazol (Qiagen) for
438 evaluation of immune responses by RNAseq. To generate localised infection, 200 cfu *M. marinum*
439 in a volume of 1 nl were injected into the hindbrain ventricle (HBV) of two dpf zebrafish larvae.
440 Cellular recruitment was evaluated by fluorescence microscopy at 6-18 hours post-infection.

441 **Tailfin transection**

442 Tailfin transections were performed as described previously *(26, 78)*. Briefly, live anaesthetised three
443 dpf zebrafish larvae were transferred with a 1 ml Pasteur pipette (Scientific Laboratory Supplies) to
444 a sterile petri dish containing 2% agarose (Bioline). Transections of the caudal fin were performed
445 using a sterile microscalpel (World Precision Instruments) by applying steady downward pressure to
446 create the incision at the boundary with the notochord. Following injury, larvae were rinsed in egg
447 water, and maintained in individual wells of a 96-well tissue culture plate (TPP) at 28.5°C until live
448 imaging to quantify neutrophil or macrophage recruitment to the site of injury at 1, 6 and 24 hours-
449 post-wound (hpw).

450 **Fluorescence microscopy**

451 All fluorescence microscopy was performed on live, anasethised larvae. For quantitation of bacterial
452 burden and dissemination four days post-infection, steady state neutrophil numbers at two dpf and
453 cellular recruitment at 2-4 dpf, larvae were imaged using an M205FA stereofluorescence microscope
454 (Leica) with a 1x objective. Larvae were imaged on a flat 1% agarose plate for quantitation of severity
455 of mycobacterial infection and steady state neutrophil numbers and a 96-well tissue culture plate
456 (TPP) in which the wells were coated with 1% agarose, for cellular recruitment to tailfin transection.
457 Micro-wells were created in 1% agarose using a Stampwell Larvae 1 device (Idylle) for optimal
458 positioning of 2-3 dpf larvae for imaging of cellular recruitment to hindbrain ventricle *M. marinum*
459 infection. Brightfield and fluorescence images were captured using a DFC365 FX camera (Leica)
460 and exported as 16-bit Tagged Image Format (TIF) files for analysis. For quantitation of steady state
461 macrophage numbers three dpf larvae were imaged in 96-well alignment plates (Funakoshi)
462 containing 75 µl egg water per well using a high-content wide-field fluorescence microscope
463 (Hermes, IDEA Bio-Medical) with a 4x objective, capturing five z planes 50.6 µm apart in four

464 contiguous fields of view per embryo. We created an ImageJ macro to semi-automate generation of
465 single maximum intensity projection z-stack montages from the Hermes images, which were saved
466 as 16-bit TIF files for analysis (Table S4. Mxa reporter expression was recorded with an EVOS
467 M7000 microscope (ThermoFisher) equipped with a 2x/NA0.06 objective and Texas Red
468 fluorescence cube. Larvae were positioned laterally in micro-wells created in 2% agarose with an in-
469 house-printed stamp. A single fluorescence plane was recorded as the depth of field is sufficient to
470 capture the entire larva. Transmitted light images were also recorded and both were exported as 16-
471 bit TIF files.

472 **Image analysis**

473 To quantify bacterial burden, number of bacterial foci and spatial distribution of bacteria, images
474 were analysed using custom QuantiFish software, previously developed in our group, to enable rapid
475 quantitation of fluorescent foci in zebrafish larvae *(79)*. Mxa reporter fluorescence was measured
476 with ImageJ. Transmitted and fluorescence images were stacked. Images were slightly rotated to
477 horizontality where necessary. A 600x100 pixel rectangular region of interest was defined on the
478 transmitted light image to encompass the entire gut and liver areas. Mean fluorescence intensity was
479 then measured on the fluorescence image. For quantitation of total cell number and recruitment of
480 fluorescent immune cells to the site of tailfin transection we developed a new custom Python script
481 which enables quantitation of integrated fluorescence within concentric zones (known as Sholl
482 circles) *(80)*. To achieve this, the script leverages the OpenCV, NumPy *(81)*, Matplotlib, SciPy
483 (http://www.scipy.org), scikit-image *(82)* and pandas Python libraries to facilitate image processing
484 and data extraction (Table S5. First the user is prompted to select a folder containing images for
485 analysis, as well as the file extensions corresponding to the brightfield and fluorescence images,
486 which are essential for the subsequent steps. The script then iterates through each pair of brightfield
487 and fluorescent images prompting the user to define two points on the brightfield image, which serve
488 as the start and end positions between which to create concentric circular regions *(80)* on the
489 corresponding fluorescence image. The script employs the image processing techniques described
490 in Table S5 to quantify integrated fluorescence of the entire image and that within each region, as a
491 surrogates for the total number of immune cells and the number at each spatial location, respectively
492 and generates output files containing this information. Integrated fluorescence within the first zone
493 (the wound site) and distance from the site of tailfin transection of the zone in which the maximal
494 integrated fluorescence (a surrogate for the highest cell numbers) was detected (identified manually)
495 were used as measures of immune cell recruitment for each zebrafish larva. The number of cells
496 recruited to the site of hindbrain *M. marinum* infection was quantified by manual counting.

497 **Genotyping by next generation sequencing**

498 ***Genomic DNA extraction***

499 Genomic DNA was extracted from anasethetised individual zebrafish larvae using the modified hot
500 sodium hydroxide and Tris (HotSHOT) method as previously described *(73, 83)*. Briefly, larvae in
501 96-well plates were incubated in 50 µl base solution (25 mM KOH, 0.2 mM EDTA in water) at 95°C
502 for 30 min then cooled to room temperature, before addition of 50 µl neutralization solution (40 mM
503 Tris-HCL in water).

504 ***PCR***

505 Extracted DNA (2 µl per 50 µl reaction) was subjected to PCR using Phusion High-Fidelity DNA
506 Polymerase (New England Biolabs) (98°C for 30 seconds (s), once only, 40 cycles of 98°C for 10 s,
507 59°C for 30 s, 72°C for 20 s, 72°C for 10 minutes, once only). Sequences and genomic positions of
508 the primers used are provided in Table S3. Successful amplification of a single product of
509 approximately 300 bp was verified by 2% agarose (Bioline) Tris-borate-EDTA (TBE) containing
510 Redsafe (Chembio) gel electrophoresis. PCR products were purified using ExoSAP-IT Express
511 (ThermoFisher), concentration of purified DNA determined by Nanodrop spectrophotometer
512 (ThermoFisher) and samples diluted to 15-25 ng/µl for sequencing.

513 ***Next generation sequencing and data analysis***

514 Sequencing was performed by the UCL Fish Genomic Service using the MiSeq Reagent Kit v2 (300-
515 cycles) (Illumina) and the MiSeq system (Illumina) in paired end mode, according to the
516 manufacturer's instructions. Sequencing data were received as two FASTQ files (forward and

517 reverse) for each sample. Visual sequence analysis was performed using Geneious 10.2.6
518 (https://www.geneious.com) for initial verification of successful genome editing close to the PAM site.
519 Objective quantitation of the proportion of reads mutated and predicted to be frameshifted was
520 achieved using the ampliCan R package *(84)*, which utilizes the FASTQ files and a metadata file
521 providing the amplicon, protospacer adjacent motif (PAM) and primer sequences (Table S3) and
522 sample information, as previously described *(73)*. AmpliCan was run with default parameters, with
523 the exception that min_freq = 0.005 (mutations at a frequency below this threshold were considered
524 a sequencing error) and average_quality = 25. Mutations present in uninjected or scrambled RNP
525 injected control samples were not included as Cas9 induced mutations.

526 **Statistical analysis**

527 Statistical analysis was performed using GraphPad Prism 9.3.1 for Windows (GraphPad Software)
528 and R3.6.3. Chi-squared tests were used to identify outlier genes statistically enriched in
529 transcriptomic data from TST samples compared to saline samples, with no correction for multiple
530 testing to avoid type 2 error. Spearman rank correlation was used to determine the strength of
531 relationship between TST transcriptome gene expression and TB disease severity (two-tailed),
532 transcript levels of upstream regulator target gene modules and TST random gene modules (one-
533 tailed, positive correlation only) and mean expression of transcriptional modules in TST
534 transcriptomic data with severity of TB disease (two-tailed). The Benjamini-Hochberg correction
535 method for multiple comparisons was used to identify upstream regulator target gene modules with
536 average correlation coefficients significantly higher than the mean of the distribution of equivalent
537 sized randomly selected gene modules by ≥2 SD (Z score ≥2) with false discovery rate <0.05.
538 Survival of *stat2* CRISPant and control zebrafish larvae was compared using a log-rank (Mantel-
539 Cox) test; a p value <0.05 was considered significant. On scatter plots horizontal lines represent
540 median values and error bars indicate the interquartile range. On box and whisker plots horizontal
541 lines represent median values, box limits indicate the interquartile range and whiskers extend
542 between the 5th and 95th percentiles of the data. Two-tailed Mann-Whitney tests were used for two
543 group comparisons of unpaired data; a p value <0.05 was considered significant. Where p values
544 are not presented on graphs, * denotes p<0.05.

545 **REFERENCES AND NOTES**

546 1. A. K. Coussens, S. M. A. Zaidi, B. W. Allwood, P. K. Dewan, G. Gray, M. Kohli, T. Kredo, B. J.
547 Marais, G. B. Marks, L. Martinez, M. Ruhwald, T. J. Scriba, J. A. Seddon, P. Tisile, D. F. Warner, R.
548 J. Wilkinson, H. Esmail, R. M. G. J. Houben, International Consensus for Early TB (ICE-TB) group,
549 Classification of early tuberculosis states to guide research for improved care and prevention: an
550 international Delphi consensus exercise. *Lancet Respir. Med.* **12**, 484–498 (2024).

551 2. A. M. Cadena, S. M. Fortune, J. L. Flynn, Heterogeneity in tuberculosis. *Nat. Rev. Immunol.* **17**,
552 691–702 (2017).

553 3. S. H. E. Kaufmann, C. Lange, M. Rao, K. N. Balaji, M. Lotze, M. Schito, A. I. Zumla, M. Maeurer,
554 Progress in tuberculosis vaccine development and host-directed therapies--a state of the art review.
555 *Lancet Respir. Med.* **2**, 301–320 (2014).

556 4. G. S. Tomlinson, T. J. Cashmore, P. T. G. Elkington, J. Yates, R. J. Lehloenya, J. Tsang, M.
557 Brown, R. F. Miller, K. Dheda, D. R. Katz, B. M. Chain, M. Noursadeghi, Transcriptional profiling of
558 innate and adaptive human immune responses to mycobacteria in the tuberculin skin test. *Eur. J.*
559 *Immunol.* **41**, 3253–3260 (2011).

560 5. L. C. K. Bell, G. Pollara, M. Pascoe, G. S. Tomlinson, R. J. Lehloenya, J. Roe, R. Meldau, R. F.
561 Miller, A. Ramsay, B. M. Chain, K. Dheda, M. Noursadeghi, In Vivo Molecular Dissection of the
562 Effects of HIV-1 in Active Tuberculosis. *PLoS Pathog.* **12**, e1005469 (2016).

563 6. M.-J. Kim, H. C. Wainwright, M. Locketz, L.-G. Bekker, G. B. Walther, C. Dittrich, A. Visser, W.
564 Wang, F.-F. Hsu, U. Wiehart, L. Tsenova, G. Kaplan, D. G. Russell, Caseation of human tuberculosis
565 granulomas correlates with elevated host lipid metabolism. *EMBO Mol. Med.* **2**, 258–274 (2010).

566 7. L. Ramakrishnan, The zebrafish guide to tuberculosis immunity and treatment. *Cold Spring Harb.*

567 *Symp. Quant. Biol.* **78**, 179–192 (2013).

568 8. G. Pollara, C. T. Turner, J. Rosenheim, A. Chandran, L. C. K. Bell, A. Khan, A. Patel, L. F. Peralta,
569 A. Folino, A. Akarca, C. Venturini, T. Baker, S. Ecker, F. L. M. Ricciardolo, T. Marafioti, C. Ugarte-
570 Gil, D. A. J. Moore, B. M. Chain, G. S. Tomlinson, M. Noursadeghi, Exaggerated IL-17A activity in
571 human in vivo recall responses discriminates active tuberculosis from latent infection and cured
572 disease. *Sci. Transl. Med.* **13**, eabg7673 (2021).

573 9. A. P. Ralph, M. Ardian, A. Wiguna, G. P. Maguire, N. G. Becker, G. Drogumuller, M. J. Wilks, G.
574 Waramori, E. Tjitra, null Sandjaja, E. Kenagalem, G. J. Pontororing, N. M. Anstey, P. M. Kelly, A
575 simple, valid, numerical score for grading chest x-ray severity in adult smear-positive pulmonary
576 tuberculosis. *Thorax* **65**, 863–869 (2010).

577 10. D. L. Roden, G. W. Sewell, A. Lobley, A. P. Levine, A. M. Smith, A. W. Segal, ZODET: software
578 for the identification, analysis and visualisation of outlier genes in microarray expression data. *PloS*
579 *One* **9**, e81123 (2014).

580 11. A. Chandran, J. Rosenheim, G. Nageswaran, L. Swadling, G. Pollara, R. K. Gupta, A. R. Burton,
581 J. A. Guerra-Assunção, A. Woolston, T. Ronel, C. Pade, J. M. Gibbons, B. Sanz-Magallon Duque
582 De Estrada, M. Robert de Massy, M. Whelan, A. Semper, T. Brooks, D. M. Altmann, R. J. Boyton,
583 Á. McKnight, G. Captur, C. Manisty, T. A. Treibel, J. C. Moon, G. S. Tomlinson, M. K. Maini, B. M.
584 Chain, M. Noursadeghi, COVIDsortium Investigators, Rapid synchronous type 1 IFN and virus-
585 specific T cell responses characterize first wave non-severe SARS-CoV-2 infections. *Cell Rep. Med.*
586 **3**, 100557 (2022).

587 12. R. L. Kinsella, D. X. Zhu, G. A. Harrison, A. E. Mayer Bridwell, J. Prusa, S. M. Chavez, C. L.
588 Stallings, Perspectives and Advances in the Understanding of Tuberculosis. *Annu. Rev. Pathol.*
589 *Mech. Dis.* **16**, 377–408 (2021).

590 13. F. Paduano, E. Gaudio, A. A. Mensah, S. Pinton, F. Bertoni, F. Trapasso, T-Cell
591 Leukemia/Lymphoma 1 (TCL1): An Oncogene Regulating Multiple Signaling Pathways. *Front.*
592 *Oncol.* **8**, 317 (2018).

593 14. F. McNab, K. Mayer-Barber, A. Sher, A. Wack, A. O'Garra, Type I interferons in infectious
594 disease. *Nat. Rev. Immunol.* **15**, 87–103 (2015).

595 15. C. Langevin, E. Aleksejeva, G. Passoni, N. Palha, J.-P. Levraud, P. Boudinot, The antiviral innate
596 immune response in fish: evolution and conservation of the IFN system. *J. Mol. Biol.* **425**, 4904–
597 4920 (2013).

598 16. J.-P. Levraud, L. Jouneau, V. Briolat, V. Laghi, P. Boudinot, IFN-Stimulated Genes in Zebrafish
599 and Humans Define an Ancient Arsenal of Antiviral Immunity. *J. Immunol. Baltim. Md 1950* **203**,
600 3361–3373 (2019).

601 17. K. Blaszczyk, H. Nowicka, K. Kostyrko, A. Antonczyk, J. Wesoly, H. A. R. Bluyssen, The unique
602 role of STAT2 in constitutive and IFN-induced transcription and antiviral responses. *Cytokine Growth*
603 *Factor Rev.* **29**, 71–81 (2016).

604 18. A. Begitt, M. Droescher, T. Meyer, C. D. Schmid, M. Baker, F. Antunes, K.-P. Knobeloch, M. R.
605 Owen, R. Naumann, T. Decker, U. Vinkemeier, STAT1-cooperative DNA binding distinguishes type
606 1 from type 2 interferon signaling. *Nat. Immunol.* **15**, 168–176 (2014).

607 19. J. W. Schoggins, Interferon-Stimulated Genes: What Do They All Do? *Annu. Rev. Virol.* **6**, 567–
608 584 (2019).

609 20. H. Clay, J. M. Davis, D. Beery, A. Huttenlocher, S. E. Lyons, L. Ramakrishnan, Dichotomous role
610 of the macrophage in early Mycobacterium marinum infection of the zebrafish. *Cell Host Microbe* **2**,
611 29–39 (2007).

612 21. A. J. Pagán, C.-T. Yang, J. Cameron, L. E. Swaim, F. Ellett, G. J. Lieschke, L. Ramakrishnan,
613 Myeloid Growth Factors Promote Resistance to Mycobacterial Infection by Curtailing Granuloma
614 Necrosis through Macrophage Replenishment. *Cell Host Microbe* **18**, 15–26 (2015).

615 22. R. D. Berg, S. Levitte, M. P. O'Sullivan, S. M. O'Leary, C. J. Cambier, J. Cameron, K. K. Takaki,
616 C. B. Moens, D. M. Tobin, J. Keane, L. Ramakrishnan, Lysosomal Disorders Drive Susceptibility to
617 Tuberculosis by Compromising Macrophage Migration. *Cell* **165**, 139–152 (2016).

618 23. C.-T. Yang, C. J. Cambier, J. M. Davis, C. J. Hall, P. S. Crosier, L. Ramakrishnan, Neutrophils
619 exert protection in the early tuberculous granuloma by oxidative killing of mycobacteria
620 phagocytosed from infected macrophages. *Cell Host Microbe* **12**, 301–312 (2012).

621 24. P. M. Elks, S. Brizee, M. van der Vaart, S. R. Walmsley, F. J. van Eeden, S. A. Renshaw, A. H.
622 Meijer, Hypoxia inducible factor signaling modulates susceptibility to mycobacterial infection via a
623 nitric oxide dependent mechanism. *PLoS Pathog.* **9**, e1003789 (2013).

624 25. I. Rauch, M. Müller, T. Decker, The regulation of inflammation by interferons and their STATs.
625 *JAK-STAT* **2**, e23820 (2013).

626 26. S. A. Renshaw, C. A. Loynes, D. M. I. Trushell, S. Elworthy, P. W. Ingham, M. K. B. Whyte, A
627 transgenic zebrafish model of neutrophilic inflammation. *Blood* **108**, 3976–3978 (2006).

628 27. C. Gray, C. A. Loynes, M. K. B. Whyte, D. C. Crossman, S. A. Renshaw, T. J. A. Chico,
629 Simultaneous intravital imaging of macrophage and neutrophil behaviour during inflammation using
630 a novel transgenic zebrafish. *Thromb. Haemost.* **105**, 811–819 (2011).

631 28. F. Ellett, L. Pase, J. W. Hayman, A. Andrianopoulos, G. J. Lieschke, mpeg1 promoter transgenes
632 direct macrophage-lineage expression in zebrafish. *Blood* **117**, e49-56 (2011).

633 29. M. P. R. Berry, C. M. Graham, F. W. McNab, Z. Xu, S. A. A. Bloch, T. Oni, K. A. Wilkinson, R.
634 Banchereau, J. Skinner, R. J. Wilkinson, C. Quinn, D. Blankenship, R. Dhawan, J. J. Cush, A. Mejias,
635 O. Ramilo, O. M. Kon, V. Pascual, J. Banchereau, D. Chaussabel, A. O'Garra, An interferon-
636 inducible neutrophil-driven blood transcriptional signature in human tuberculosis. *Nature* **466**, 973–
637 977 (2010).

638 30. C. I. Bloom, C. M. Graham, M. P. R. Berry, K. A. Wilkinson, T. Oni, F. Rozakeas, Z. Xu, J.
639 Rossello-Urgell, D. Chaussabel, J. Banchereau, V. Pascual, M. Lipman, R. J. Wilkinson, A. O'Garra,
640 Detectable Changes in The Blood Transcriptome Are Present after Two Weeks of Antituberculosis
641 Therapy. *PLOS ONE* **7**, e46191 (2012).

642 31. T. H. M. Ottenhoff, R. H. Dass, N. Yang, M. M. Zhang, H. E. E. Wong, E. Sahiratmadja, C. C.
643 Khor, B. Alisjahbana, R. van Crevel, S. Marzuki, M. Seielstad, E. van de Vosse, M. L. Hibberd,
644 Genome-Wide Expression Profiling Identifies Type 1 Interferon Response Pathways in Active
645 Tuberculosis. *PLOS ONE* **7**, e45839 (2012).

646 32. K. D. Mayer-Barber, B. B. Andrade, D. L. Barber, S. Hieny, C. G. Feng, P. Caspar, S. Oland, S.
647 Gordon, A. Sher, Innate and Adaptive Interferons Suppress IL-1α and IL-1β Production by Distinct
648 Pulmonary Myeloid Subsets during Mycobacterium tuberculosis Infection. *Immunity* **35**, 1023–1034
649 (2011).

650 33. K. D. Mayer-Barber, B. B. Andrade, S. D. Oland, E. P. Amaral, D. L. Barber, J. Gonzales, S. C.
651 Derrick, R. Shi, N. P. Kumar, W. Wei, X. Yuan, G. Zhang, Y. Cai, S. Babu, M. Catalfamo, A. M.
652 Salazar, L. E. Via, C. E. Barry, A. Sher, Host-directed therapy of tuberculosis based on interleukin-
653 1 and type I interferon crosstalk. *Nature* **511**, 99–103 (2014).

654 34. D. X. Ji, L. H. Yamashiro, K. J. Chen, N. Mukaida, I. Kramnik, K. H. Darwin, R. E. Vance, Type I
655 interferon-driven susceptibility to Mycobacterium tuberculosis is mediated by IL-1Ra. *Nat. Microbiol.*
656 **4**, 2128–2135 (2019).

657 35. D. I. Kotov, O. V. Lee, S. A. Fattinger, C. A. Langner, J. V. Guillen, J. M. Peters, A. Moon, E. M.
658 Burd, K. C. Witt, D. B. Stetson, D. L. Jaye, B. D. Bryson, R. E. Vance, Early cellular mechanisms of
659 type I interferon-driven susceptibility to tuberculosis. *Cell* **186**, 5536-5553.e22 (2023).

660 36. L. Moreira-Teixeira, K. Mayer-Barber, A. Sher, A. O'Garra, Type I interferons in tuberculosis: Foe
661 and occasionally friend. *J. Exp. Med.* **215**, 1273–1285 (2018).

662 37. I. Kramnik, G. Beamer, Mouse models of human TB pathology: roles in the analysis of necrosis
663 and the development of host-directed therapies. *Semin. Immunopathol.* **38**, 221–237 (2016).

664 38. S. Giosué, M. Casarini, L. Alemanno, G. Galluccio, P. Mattia, G. Pedicelli, L. Rebek, A. Bisetti,
665 F. Ameglio, Effects of aerosolized interferon-alpha in patients with pulmonary tuberculosis. *Am. J.*
666 *Respir. Crit. Care Med.* **158**, 1156–1162 (1998).

667 39. P. Zarogoulidis, I. Kioumis, N. Papanas, K. Manika, T. Kontakiotis, A. Papagianis, K.
668 Zarogoulidis, The effect of combination IFN-alpha-2a with usual antituberculosis chemotherapy in
669 non-responding tuberculosis and diabetes mellitus: a case report and review of the literature. *J.*
670 *Chemother.* **24**, 173–177 (2012).

671 40. D. Mansoori, S. Tavana, M. Mirsaeidi, M. Yazdanpanah, H. Sohrabpour, The Efficacy of
672 Interferon-α in the Treatment of Multidrug Resistant Tuberculosis. *TANAFFOS* **1**, 29–34 (2002).

673 41. Y. E. Liu, P. A. Darrah, J. J. Zeppa, M. Kamath, F. Laboune, D. C. Douek, P. Maiello, M.
674 Roederer, J. L. Flynn, R. A. Seder, P. Khatri, Blood transcriptional correlates of BCG-induced
675 protection against tuberculosis in rhesus macaques. *Cell Rep. Med.* **4**, 101096 (2023).

676 42. L. B. Tezera, M. K. Bielecka, A. Chancellor, M. T. Reichmann, B. A. Shammari, P. Brace, A.
677 Batty, A. Tocheva, S. Jogai, B. G. Marshall, M. Tebruegge, S. N. Jayasinghe, S. Mansour, P. T.
678 Elkington, B. Aldridge, Ed. Dissection of the host-pathogen interaction in human tuberculosis using
679 a bioengineered 3-dimensional model. *eLife* **6**, e21283 (2017).

680 43. V. Torraca, C. Cui, R. Boland, J.-P. Bebelman, A. M. van der Sar, M. J. Smit, M. Siderius, H. P.
681 Spaink, A. H. Meijer, The CXCR3-CXCL11 signaling axis mediates macrophage recruitment and
682 dissemination of mycobacterial infection. *Dis. Model. Mech.* **8**, 253–269 (2015).

683 44. J. M. Davis, H. Clay, J. L. Lewis, N. Ghori, P. Herbomel, L. Ramakrishnan, Real-time visualization
684 of mycobacterium-macrophage interactions leading to initiation of granuloma formation in zebrafish
685 embryos. *Immunity* **17**, 693–702 (2002).

686 45. D. M. Tobin, F. J. Roca, S. F. Oh, R. McFarland, T. W. Vickery, J. P. Ray, D. C. Ko, Y. Zou, N.
687 D. Bang, T. T. H. Chau, J. C. Vary, T. R. Hawn, S. J. Dunstan, J. J. Farrar, G. E. Thwaites, M.-C.
688 King, C. N. Serhan, L. Ramakrishnan, Host genotype-specific therapies can optimize the
689 inflammatory response to mycobacterial infections. *Cell* **148**, 434–446 (2012).

690 46. A.-L. Neehus, B. Carey, M. Landekic, P. Panikulam, G. Deutsch, M. Ogishi, C. A. Arango-Franco,
691 Q. Philippot, M. Modaresi, I. Mohammadzadeh, M. Corcini Berndt, D. Rinchai, T. Le Voyer, J. Rosain,
692 M. Momenilandi, M. Martin-Fernandez, T. Khan, J. Bohlen, J. E. Han, A. Deslys, M. Bernard, T.
693 Gajardo-Carrasco, C. Soudée, C. Le Floc'h, M. Migaud, Y. Seeleuthner, M.-S. Jang, E. Nikolouli, S.
694 Seyedpour, H. Begueret, J.-F. Emile, P. Le Guen, G. Tavazzi, C. N. J. Colombo, F. C. Marzani, M.
695 Angelini, F. Trespidi, S. Ghirardello, N. Alipour, A. Molitor, R. Carapito, M. Mazloomrezaei, H. Rokni-
696 Zadeh, M. Changi-Ashtiani, C. Brouzes, P. Vargas, A. Borghesi, N. Lachmann, S. Bahram, B.
697 Crestani, S. Pahari, L. S. Schlesinger, N. Marr, D. Bugonovic, S. Boisson-Dupuis, V. Béziat, L. Abel,
698 R. Borie, L. R. Young, R. Deterding, M. Shahrooei, N. Rezaei, N. Parvaneh, D. Craven, P. Gros, D.
699 Malo, F. E. Sepulveda, L. M. Nogee, N. Aladjidi, B. C. Trapnell, J.-L. Casanova, J. Bustamante,
700 Human inherited CCR2 deficiency underlies progressive polycystic lung disease. *Cell* **187**, 390-
701 408.e23 (2024).

702 47. K. B. Walters, J. M. Green, J. C. Surfus, S. K. Yoo, A. Huttenlocher, Live imaging of neutrophil

703 motility in a zebrafish model of WHIM syndrome. *Blood* **116**, 2803–2811 (2010).

704 48. M. H. Lehmann, L. E. Torres-Domínguez, P. J. R. Price, C. Brandmüller, C. J. Kirschning, G.
705 Sutter, CCL2 expression is mediated by type I IFN receptor and recruits NK and T cells to the lung
706 during MVA infection. *J. Leukoc. Biol.* **99**, 1057–1064 (2016).

707 49. M. Buttmann, C. Merzyn, P. Rieckmann, Interferon-beta induces transient systemic IP-
708 10/CXCL10 chemokine release in patients with multiple sclerosis. *J. Neuroimmunol.* **156**, 195–203
709 (2004).

710 50. C. J. Cambier, K. K. Takaki, R. P. Larson, R. E. Hernandez, D. M. Tobin, K. B. Urdahl, C. L.
711 Cosma, L. Ramakrishnan, Mycobacteria manipulate macrophage recruitment through coordinated
712 use of membrane lipids. *Nature* **505**, 218–222 (2014).

713 51. L. Abel, J. Fellay, D. W. Haas, E. Schurr, G. Srikrishna, M. Urbanowski, N. Chaturvedi, S.
714 Srinivasan, D. H. Johnson, W. R. Bishai, Genetics of human susceptibility to active and latent
715 tuberculosis: present knowledge and future perspectives. *Lancet Infect. Dis.* **18**, e64–e75 (2018).

716 52. A. Khadela, V. P. Chavda, H. Postwala, Y. Shah, P. Mistry, V. Apostolopoulos, Epigenetics in
717 Tuberculosis: Immunomodulation of Host Immune Response. *Vaccines* **10**, 1740 (2022).

718 53. A. L. Jacobs, Infective dose in pulmonary tuberculosis. *Tubercle* **22**, 266–271 (1941).

719 54. C. R. Plumlee, F. J. Duffy, B. H. Gern, J. L. Delahaye, S. B. Cohen, C. R. Stoltzfus, T. R. Rustad,
720 S. G. Hansen, M. K. Axthelm, L. J. Picker, J. D. Aitchison, D. R. Sherman, V. V. Ganusov, M. Y.
721 Gerner, D. E. Zak, K. B. Urdahl, Ultra-low Dose Aerosol Infection of Mice with Mycobacterium
722 tuberculosis More Closely Models Human Tuberculosis. *Cell Host Microbe* **29**, 68-82.e5 (2021).

723 55. J.-L. Casanova, M. S. Anderson, Unlocking life-threatening COVID-19 through two types of
724 inborn errors of type I IFNs. *J. Clin. Invest.* **133**, e166283.

725 56. P. Elkington, T. Shiomi, R. Breen, R. K. Nuttall, C. A. Ugarte-Gil, N. F. Walker, L. Saraiva, B.
726 Pedersen, F. Mauri, M. Lipman, D. R. Edwards, B. D. Robertson, J. D'Armiento, J. S. Friedland,
727 MMP-1 drives immunopathology in human tuberculosis and transgenic mice. *J. Clin. Invest.* **121**,
728 1827–1833 (2011).

729 57. L. Guglielmetti, A. Cazzadori, M. Conti, F. Boccafoglio, A. Vella, R. Ortolani, E. Concia,
730 Lymphocyte subpopulations in active tuberculosis: association with disease severity and the QFT-
731 GIT assay. *Int. J. Tuberc. Lung Dis. Off. J. Int. Union Tuberc. Lung Dis.* **17**, 825–828 (2013).

732 58. J. O. Jurado, V. Pasquinelli, I. B. Alvarez, D. Peña, A. I. Rovetta, N. L. Tateosian, H. E. Romeo,
733 R. M. Musella, D. Palmero, H. E. Chuluyán, V. E. García, IL-17 and IFN-γ expression in lymphocytes
734 from patients with active tuberculosis correlates with the severity of the disease. *J. Leukoc. Biol.* **91**,
735 991–1002 (2012).

736 59. Z. Hasan, B. Jamil, J. Khan, R. Ali, M. A. Khan, N. Nasir, M. S. Yusuf, S. Jamil, M. Irfan, R.
737 Hussain, Relationship between circulating levels of IFN-gamma, IL-10, CXCL9 and CCL2 in
738 pulmonary and extrapulmonary tuberculosis is dependent on disease severity. *Scand. J. Immunol.*
739 **69**, 259–267 (2009).

740 60. J. Roe, C. Venturini, R. K. Gupta, C. Gurry, B. M. Chain, Y. Sun, J. Southern, C. Jackson, M. C.
741 Lipman, R. F. Miller, A. R. Martineau, I. Abubakar, M. Noursadeghi, Blood Transcriptomic
742 Stratification of Short-term Risk in Contacts of Tuberculosis. *Clin. Infect. Dis. Off. Publ. Infect. Dis.*
743 *Soc. Am.* **70**, 731–737 (2020).

744 61. N. L. Bray, H. Pimentel, P. Melsted, L. Pachter, Near-optimal probabilistic RNA-seq
745 quantification. *Nat. Biotechnol.* **34**, 525–527 (2016).

746 62. C. Soneson, M. I. Love, M. D. Robinson, Differential analyses for RNA-seq: transcript-level
747 estimates improve gene-level inferences. *F1000Research* **4**, 1521 (2015).

748 63. S. Durinck, P. T. Spellman, E. Birney, W. Huber, Mapping identifiers for the integration of
749 genomic datasets with the R/Bioconductor package biomaRt. *Nat. Protoc.* **4**, 1184–1191 (2009).

750 64. J. T. Leek, W. E. Johnson, H. S. Parker, A. E. Jaffe, J. D. Storey, The sva package for removing
751 batch effects and other unwanted variation in high-throughput experiments. *Bioinforma. Oxf. Engl.*
752 **28**, 882–883 (2012).

753 65. H. Fang, B. Knezevic, K. L. Burnham, J. C. Knight, XGR software for enhanced interpretation of
754 genomic summary data, illustrated by application to immunological traits. *Genome Med.* **8**, 129
755 (2016).

756 66. C. T. Turner, J. Brown, E. Shaw, I. Uddin, E. Tsaliki, J. K. Roe, G. Pollara, Y. Sun, J. M. Heather,
757 M. Lipman, B. Chain, M. Noursadeghi, Persistent T Cell Repertoire Perturbation and T Cell
758 Activation in HIV After Long Term Treatment. *Front. Immunol.* **12**, 634489 (2021).

759 67. M. Jacomy, T. Venturini, S. Heymann, M. Bastian, ForceAtlas2, a continuous graph layout
760 algorithm for handy network visualization designed for the Gephi software. *PloS One* **9**, e98679
761 (2014).

762 68. W. R. Swindell, X. Xing, P. E. Stuart, C. S. Chen, A. Aphale, R. P. Nair, J. J. Voorhees, J. T.
763 Elder, A. Johnston, J. E. Gudjonsson, Heterogeneity of inflammatory and cytokine networks in
764 chronic plaque psoriasis. *PloS One* **7**, e34594 (2012).

765 69. T. Hulsen, J. de Vlieg, W. Alkema, BioVenn - a web application for the comparison and
766 visualization of biological lists using area-proportional Venn diagrams. *BMC Genomics* **9**, 488 (2008).

767 70. C. Nusslein-Volhard, *Zebrafish: A Practical Approach* R. Dahm, Ed. (Oxford University Press,
768 Oxford, 1 edition., 2002).

769 71. G. Maarifi, N. Smith, S. Maillet, O. Moncorgé, C. Chamontin, J. Edouard, F. Sohm, F. P. Blanchet,
770 J.-P. Herbeuval, G. Lutfalla, J.-P. Levraud, N. J. Arhel, S. Nisole, TRIM8 is required for virus-induced
771 IFN response in human plasmacytoid dendritic cells. *Sci. Adv.* **5**, eaax3511 (2019).

772 72. K. Voelz, R. L. Gratacap, R. T. Wheeler, A zebrafish larval model reveals early tissue-specific
773 innate immune responses to Mucor circinelloides. *Dis. Model. Mech.* **8**, 1375–1388 (2015).

774 73. F. Kroll, G. T. Powell, M. Ghosh, G. Gestri, P. Antinucci, T. J. Hearn, H. Tunbak, S. Lim, H. W.
775 Dennis, J. M. Fernandez, D. Whitmore, E. Dreosti, S. W. Wilson, E. J. Hoffman, J. Rihel, S. C. Ekker,
776 D. Y. Stainier, D. Balciunas, Eds. A simple and effective F0 knockout method for rapid screening of
777 behaviour and other complex phenotypes. *eLife* **10**, e59683 (2021).

778 74. D. Aggad, M. Mazel, P. Boudinot, K. E. Mogensen, O. J. Hamming, R. Hartmann, S. Kotenko,
779 P. Herbomel, G. Lutfalla, J.-P. Levraud, The two groups of zebrafish virus-induced interferons signal
780 via distinct receptors with specific and shared chains. *J. Immunol. Baltim. Md 1950* **183**, 3924–3931
781 (2009).

782 75. K. Takaki, J. M. Davis, K. Winglee, L. Ramakrishnan, Evaluation of the pathogenesis and
783 treatment of Mycobacterium marinum infection in zebrafish. *Nat. Protoc.* **8**, 1114–1124 (2013).

784 76. L. M. van Leeuwen, M. van der Kuip, S. A. Youssef, A. de Bruin, W. Bitter, A. M. van Furth, A.
785 M. van der Sar, Modeling tuberculous meningitis in zebrafish using Mycobacterium marinum. *Dis.*
786 *Model. Mech.* **7**, 1111–1122 (2014).

787 77. E. L. Benard, A. M. van der Sar, F. Ellett, G. J. Lieschke, H. P. Spaink, A. H. Meijer, Infection of
788 zebrafish embryos with intracellular bacterial pathogens. *J. Vis. Exp. JoVE* (2012),

789 doi:10.3791/3781.

790 78. R. N. Wilkinson, S. Elworthy, P. W. Ingham, F. J. M. van Eeden, A method for high-throughput
791 PCR-based genotyping of larval zebrafish tail biopsies. *BioTechniques* **55**, 314–316 (2013).

792 79. D. R. Stirling, O. Suleyman, E. Gil, P. M. Elks, V. Torraca, M. Noursadeghi, G. S. Tomlinson,
793 Analysis tools to quantify dissemination of pathology in zebrafish larvae. *Sci. Rep.* **10**, 3149 (2020).

794 80. D. A. Sholl, Dendritic organization in the neurons of the visual and motor cortices of the cat. *J.*
795 *Anat.* **87**, 387–406 (1953).

796 81. S. van der Walt, S. C. Colbert, G. Varoquaux, The NumPy Array: A Structure for Efficient
797 Numerical Computation. *Comput. Sci. Eng.* **13**, 22–30 (2011).

798 82. S. van der Walt, J. L. Schönberger, J. Nunez-Iglesias, F. Boulogne, J. D. Warner, N. Yager, E.
799 Gouillart, T. Yu, scikit-image contributors, scikit-image: image processing in Python. *PeerJ* **2**, e453
800 (2014).

801 83. N. D. Meeker, S. A. Hutchinson, L. Ho, N. S. Trede, Method for isolation of PCR-ready genomic
802 DNA from zebrafish tissues. *BioTechniques* **43**, 610, 612, 614 (2007).

803 84. K. Labun, X. Guo, A. Chavez, G. Church, J. A. Gagnon, E. Valen, Accurate analysis of genuine
804 CRISPR editing events with ampliCan. *Genome Res.* **29**, 843–847 (2019).

805

806 **ACKNOWLEDGEMENTS**

807 We thank Michelle Berin and Victoria Dean (Clinical Research Nurses, UCL Division of Infection and
808 Immunity) and Mylah Ramirez (Research Nurse, Barts Health NHS Trust) for support with research
809 governance, participant recruitment and sample collection. We thank the UCL Zebrafish Facility staff,
810 particularly Heather Callaway, Jenna Hakkesteeg, Karen Dunford, Carole Wilson and Elise
811 Hitchcock for maintenance of the zebrafish lines used in this study, especially during the first wave
812 of the COVID-19 pandemic. We thank UCL Genomics for library preparation and sequencing of
813 samples for transcriptional profiling (www.ucl.ac.uk/child-health/research/genetics-and-genomic-
814 medicine/ucl-genomics). We thank Alex Lubin and Katie-Jo Miller for next generation sequencing of
815 zebrafish samples for genotyping. This work has benefited from the facilities and expertise of
816 CELPHEDIA-TEFOR, UAR2010 TEFOR Paris-Saclay (TEFOR Infrastructure - Investissement
817 d'avenir - ANR-II-INBS-0014) and from the Recombinant Protein Platform of the Institut Pasteur,
818 Paris.

819 **FUNDING**

820 UK Medical Research Council Clinician Scientist Fellowship MR/N007727/1 (GST)

821 Wellcome Trust Investigator Award 207511/Z/17/Z (MN)

822 Sir Henry Dale Fellowship jointly funded by the Wellcome Trust and the Royal Society 105570/Z/14/Z
823 (PME)

824 Fondation pour la Recherche Medicale grant EQU202203014646 (J-PL)

825 National Institute of Health Research Biomedical Research Centre Funding to University College
826 Hospitals NHS Foundation Trust and University College London (GST, MN)

827 This research was funded in whole, or in part, by the Wellcome Trust [207511/Z/17/Z,
828 105570/Z/14/Z]. For the purpose of Open Access, the author has applied a CC BY public copyright
829 licence to any Author Accepted Manuscript version arising from this submission.

830 **AUTHOR CONTRIBUTIONS**

831 Conceived the study: GST, MN

832 Collected the data: ASS, BSMDDE, JR, ET, GP, J-PL, GST

Provided resources or analysis tools: ASS, BSMDDE, JR, CTT, MCIL, HK, GP, PME, EMP, J-PL, MN, GST

Performed the data analysis / interpretation: ASS, BSMDDE, JR, CTT, GP, PME, EMP, J-PL, MN, GST

Prepared the manuscript draft: GST, ASS, BSMDDE

All authors reviewed and contributed to the final manuscript.

COMPETING INTERESTS

The authors declare that they have no competing interests.

DATA AND MATERIALS AVAILABILITY

Human RNAseq data are already available in the ArrayExpress repository under accession number E-MTAB-6816. Zebrafish RNAseq data will be made available in ArrayExpress at the time of peer reviewed publication of the manuscript. The source code and manual for QuantiFish software used for analysis of bacterial burden and dissemination in zebrafish larvae are available at https://github.com/DavidStirling/QuantiFish. The ImageJ macro used to generate montages from the Hermes images and source code and manual for the Python script used for analysis of steady state cell numbers and cellular recruitment in zebrafish are available at https://github.com/AndSzyShe/particle_analysis. Source data for figure panels with fewer than 20 data points are available in Data file S1.

852 **FIGURES**

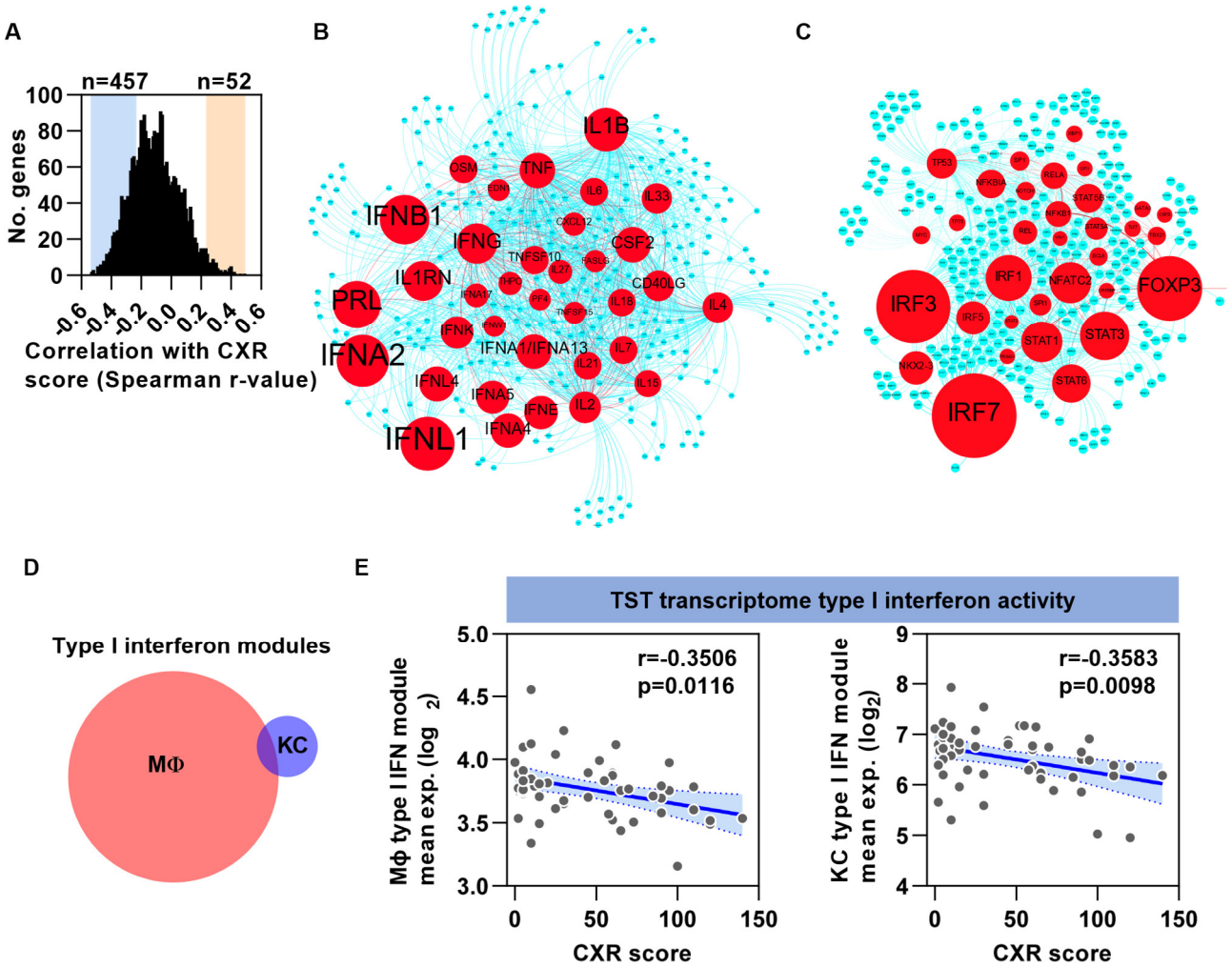

853

854 **Fig. 1. Reduced type I interferon activity in the TST transcriptome is associated with**
855 **increased severity of human TB disease. (A)** Frequency distribution of the correlation coefficients
856 for the relationship between the abundance of each of the 3222 transcripts within the tuberculin skin
857 test (TST) transcriptome derived from 51 individuals with pulmonary tuberculosis (TB) and
858 radiographic disease severity. Coloured boxes highlight statistically significant correlations ($p<0.05$).
859 **(B, C)** Network diagrams of statistically significant (FDR<0.05) cytokines **(B)** and transcription factors
860 **(C)** predicted to be upstream regulators (red) of target gene modules (blue) whose expression is
861 negatively correlated with radiological TB severity. Size of the nodes for upstream regulators is
862 proportional to -Log10 p value. Nodes were clustered using the Force Atlas 2 algorithm in Gephi
863 (version 0.9.2). **(D, E)** The inverse relationship between average expression in each TST sample of
864 two distinct, independently derived gene modules representing type I interferon activity **(D)** with TB
865 severity **(E)**. r values and p values were derived from two-tailed Spearman rank correlations. CXR =
866 Chest x-ray, MΦ = Macrophage, KC = Keratinocyte.

867
868

869

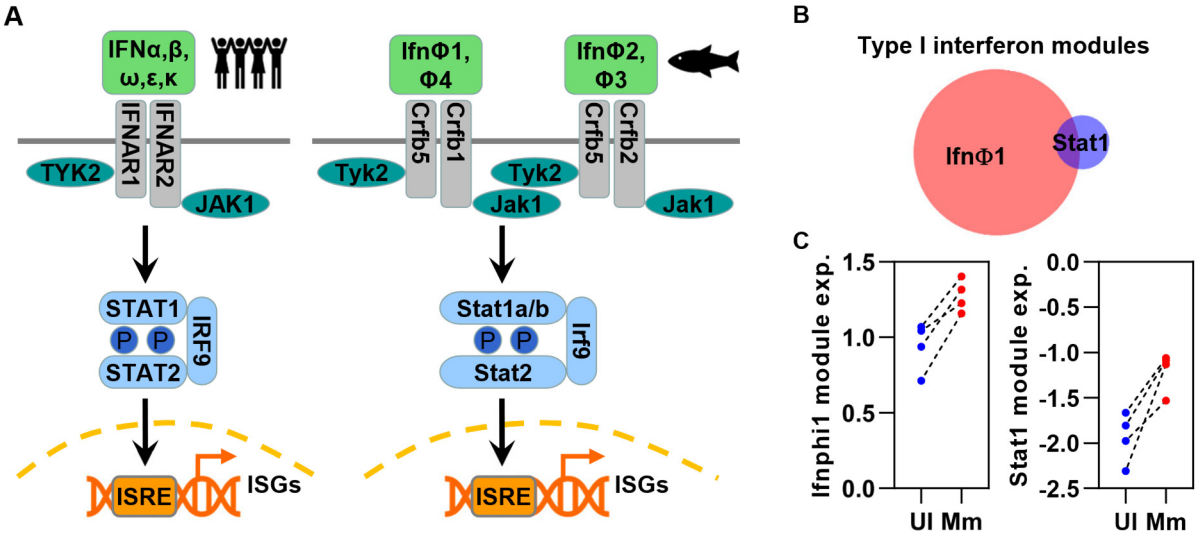

870

871 **Fig. 2. *M. marinum* infection induces a type I interferon response in zebrafish larvae.**
872 **(A)** Schematic representation of the human canonical type I interferon signalling pathway (left) which
873 is highly conserved in zebrafish (right). **(B, C)** The average expression of two largely non-overlapping
874 **(B)** type I interferon inducible gene modules derived from independent data (Table S1) is elevated
875 in *M. marinum* (Mm) infected embryos (4 days post-intravenous infection) compared with uninfected
876 (UI) siblings **(C)**. Data are from four independent experiments.

877

878

879

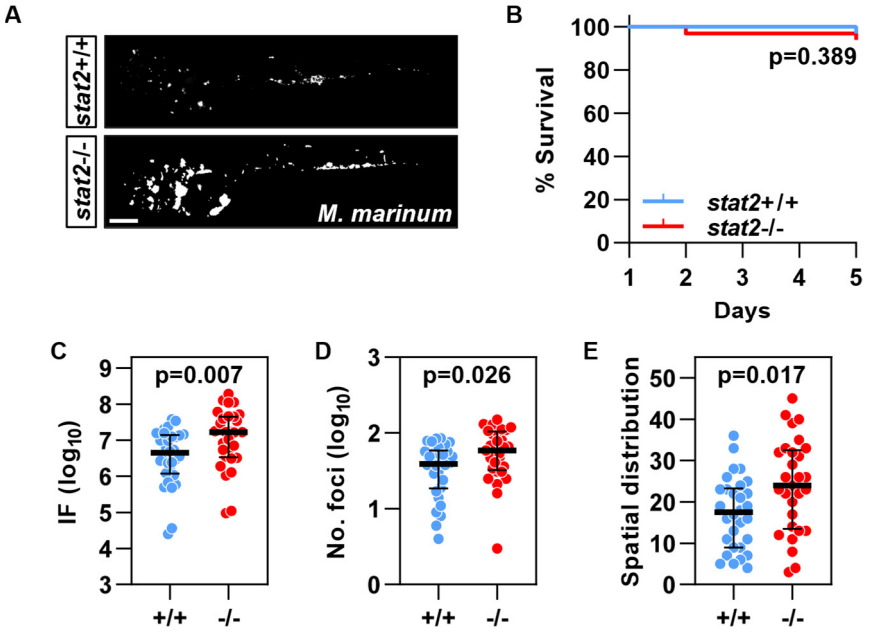

880

881 **Fig. 3. Increased severity of *M. marinum* infection in *stat2* CRISPants. (A)** *stat2* CRISPant
882 (*stat2*-/-) and control ribonucleoprotein (RNP) injected (*stat2*+/+) zebrafish larvae four days post
883 intravenous infection with 400 colony forming units (cfu) mCherry-expressing *M. marinum*. Scale bar
884 = 250 µm. **(B)** Survival of control and *stat2* disrupted zebrafish larvae 1-4 days post infection with
885 *M. marinum*. p value was derived from a log-rank (Mantel-Cox) test. **(C-E)** Comparison of integrated
886 fluorescence (IF) (a surrogate for bacterial burden) **(C)**, number of bacterial foci **(D)** and spatial
887 distribution of bacteria **(E)**, in *stat2* CRISPants compared to control RNP injected siblings. Each data
888 point represents an individual zebrafish larva, lines and error bars indicate the median and
889 interquartile range. p values were derived from two-tailed Mann-Whitney tests. Data are
890 representative of four experiments.

891

892

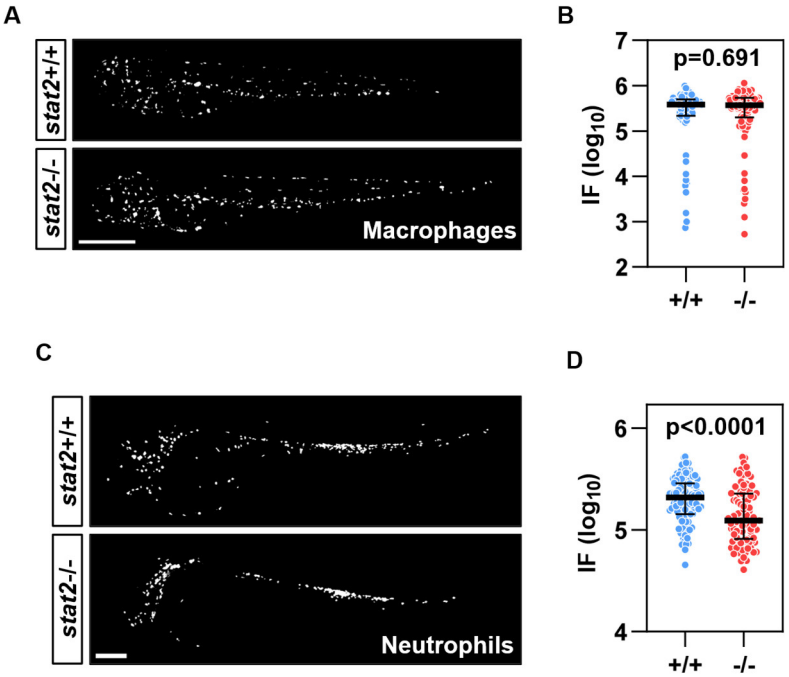

Fig. 4. Reduced steady state neutrophil numbers in *stat2* CRISPants. (A) Representative images of three day post-fertilisation (dpf) control (upper panel) and *stat2* CRISPant (lower panel) *Tg(mpeg1:mCherry)* zebrafish larvae. Scale bar = 250 µm. **(B)** Integrated fluorescence (IF) as a surrogate for steady state macrophage numbers in three dpf *stat2* CRISPants compared to siblings injected with scrambled RNPs. **(C)** Representative images of two dpf control (upper panel) and *stat2* CRISPant (lower panel) *Tg(mpx:eGFP)* zebrafish larvae. Scale bar = 250 µm. **(D)** Quantitation of baseline neutrophil numbers (represented by IF) in two dpf *stat2* CRISPants and negative control RNP injected siblings. Each data point represents an individual zebrafish larva, lines and error bars indicate the median and interquartile range. p values were derived from two-tailed Mann-Whitney tests. Data are from three independent experiments.

907

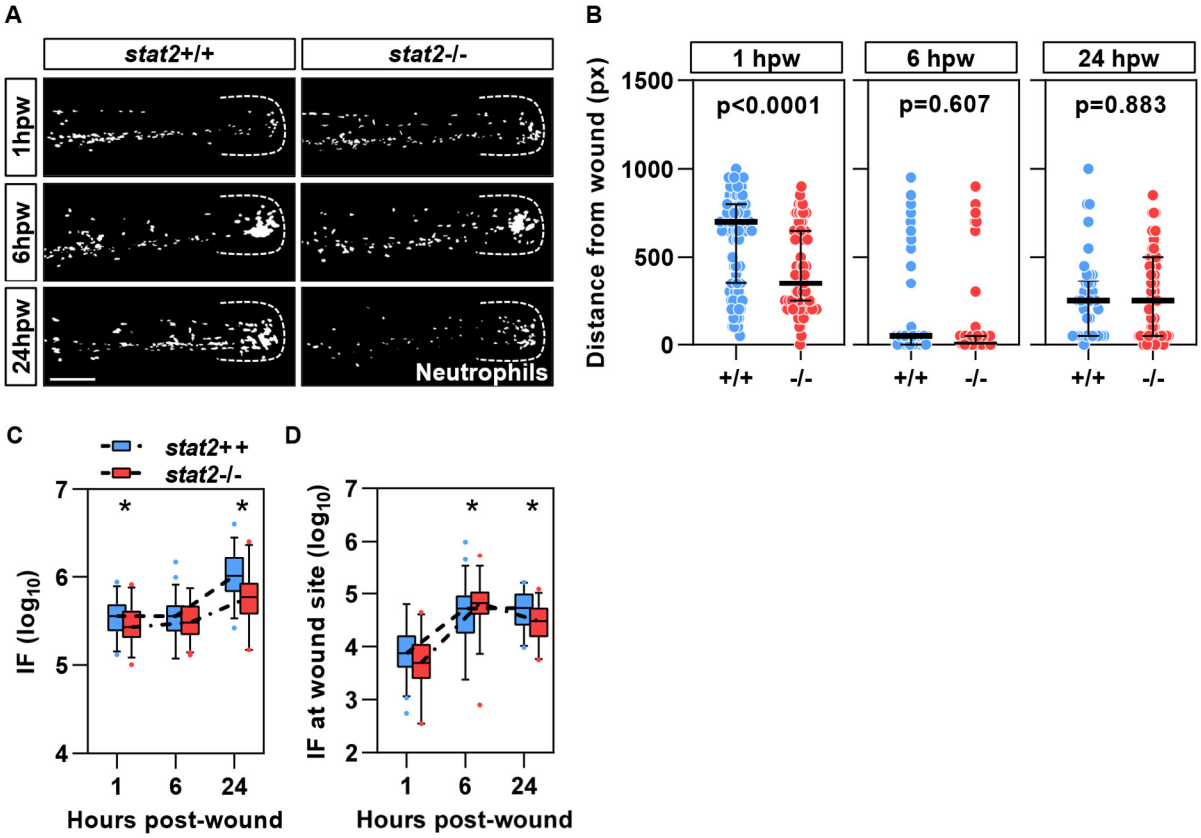

908

909 **Fig. 5. Neutrophil recruitment to the site of sterile injury is not *stat2* dependent.**
910 **(A)** Representative images of eGFP-expressing neutrophils recruited to the site of injury 1, 6 and 24
911 hours following tailfin transection of three day post-fertilisation *stat2* CRISPant *Tg(mpx:eGFP)*
912 zebrafish larvae and scrambled RNP injected controls. Scale bar represents 100 µm. **(B)** Distance
913 of neutrophils from the injury site at 1, 6 and 24 hours post-wound (hpw), derived by identifying the
914 Sholl circle in which the maximum integrated fluorescence (IF), a surrogate for highest cell numbers,
915 was detected in *stat2* CRISPants and scrambled RNP injected siblings. **(C-D)** IF, a surrogate for
916 total neutrophil numbers **(C)**, and IF at the wound site, representing neutrophil numbers localized to
917 the tailfin transection **(D)** are shown at 1, 6 and 24 hours following injury. On scatter plots data points
918 represent individual zebrafish larvae and lines and error bars the median and interquartile range. On
919 box and whisker plots horizontal lines represent median values, box limits indicate the interquartile
920 range and whiskers extend between the 5th and 95th percentiles. p values were derived from two-
921 tailed Mann-Whitney tests. * = $p<0.05$. Data are from three independent experiments. px = Pixels.

922

923

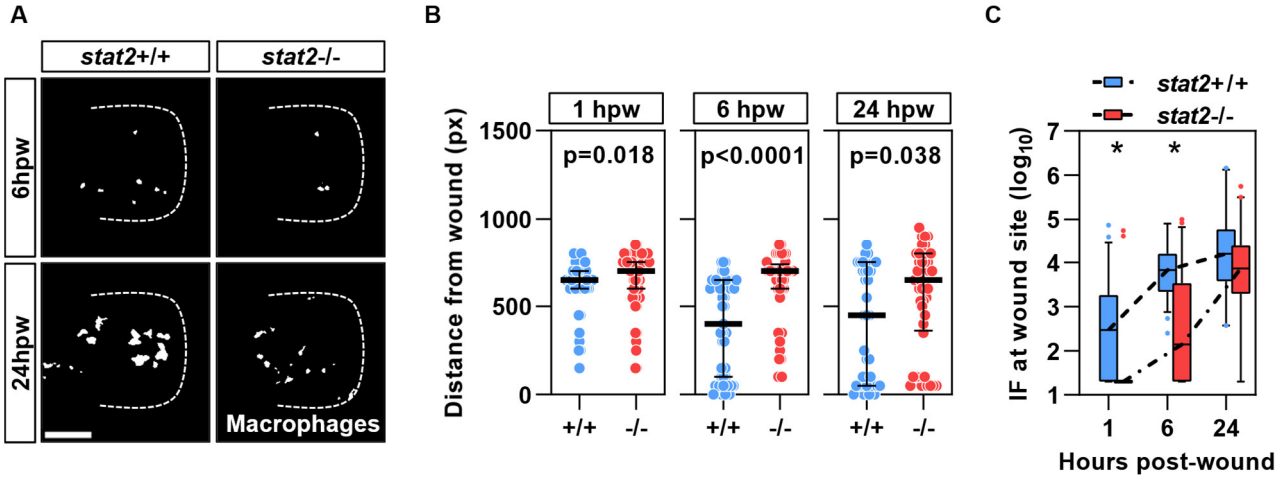

Fig. 6. Reduced macrophage recruitment to the site of sterile injury in *stat2* CRISPants. (A) Representative images of mCherry-expressing macrophages recruited to the site of tailfin transection by 6 and 24 hours, in three day post-fertilisation *stat2* CRISPant *Tg(mpeg1:mCherry)* zebrafish embryos and controls. Scale bar represents 100 µm. **(B)** Comparison of the distance of macrophages from the site of injury at the indicated time points for *stat2* CRISPants and control RNP injected siblings. **(C)** Integrated fluorescence (IF) a surrogate for macrophage numbers at the site of tailfin transection is shown at 1, 6 and 24 hours post-wound (hpw). On scatter plots data points represent individual zebrafish larvae and lines and error bars the median and interquartile range. On box and whisker plots horizontal lines represent median values, box limits indicate the interquartile range and whiskers extend between the 5th and 95th percentiles. p values were derived from two-tailed Mann-Whitney tests. * = p<0.05. Data are from three independent experiments. px = Pixels.

939

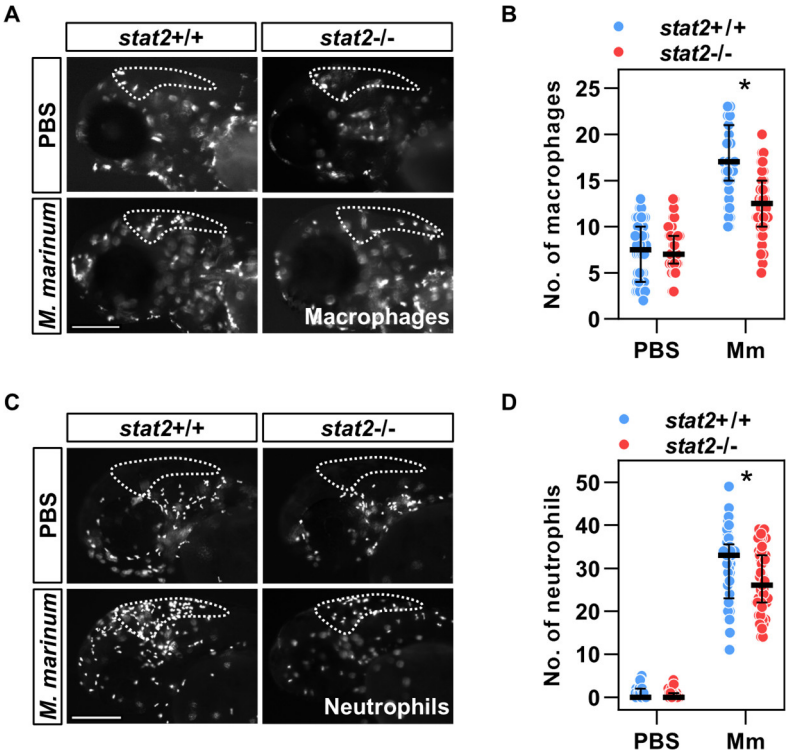

940

941 **Fig. 7. Reduced macrophage and neutrophil recruitment to *M. marinum* in *stat2* CRISPants.**
942 **(A)** Representative images of mCherry-expressing macrophages recruited to the hindbrain (dashed
943 white outline) 18 hours following injection of PBS or 200 colony forming units (cfu) *M. marinum* in
944 two day post-fertilisation (dpf) *stat2* CRISPant *Tg(mpeg1:mCherry)* zebrafish larvae and scrambled
945 ribonucleoprotein (RNP) injected controls. **(B)** Number of macrophages recruited to the hindbrain in
946 response to PBS or *M. marinum* in *stat2* CRISPants and negative control RNP injected siblings.
947 **(C)** Representative images of eGFP-expressing neutrophils recruited to the hindbrain 6 hours after
948 PBS or *M. marinum* injection (200 cfu) in two dpf *stat2* CRISPant and control *Tg(mpx:eGFP)*
949 zebrafish larvae. **(D)** Quantitation of neutrophils recruited to the site of *M. marinum* infection in *stat2*
950 CRISPants and control siblings. Scale bars represent 100 µm. Data points represent individual
951 zebrafish larvae and lines and error bars the median and interquartile range. p values were derived
952 from two-tailed Mann-Whitney tests. * = $p<0.05$. Data are from three independent experiments.

953

954

955 **TABLES**

956 **Table 1. Clinical and demographic data summary.** Demographic characteristics and magnitude
957 of clinical induration at the site of TST or saline injection are summarised for all study subjects.
958 Duration of anti-tuberculous drug treatment at the time of sampling and radiographic disease severity
959 data are provided for individuals with pulmonary TB. Saline samples were obtained from 17
960 individuals with pulmonary TB and 32 healthy participants who were people with cured or latent TB,
961 BCG vaccine recipients and healthy volunteers, described previously *(8)*. CXR = chest x-ray.
962 *Applies only to participants with active TB receiving saline injections.

		TST	Saline
Number		51	49
Age	(median and range)	30 (19-77)	28 (18-75)
Sex	Male	31 (61%)	19 (39%)
	Female	20 (39%)	30 (61%)
Ethnicity	White	21 (41%)	20 (41%)
	Asian	15 (29%)	8 (16%)
	Black	12 (24%)	7 (14%)
	Mixed	2 (4%)	1 (2%)
	South American	1 (2%)	11 (22%)
	Not recorded	NA	2 (4%)
Injection site induration (mm)	(median and range)	20 (0-70)	0
Days TB treatment before TST +/ saline	(median and range)	19 (0-30)	15 (0-28)*
CXR severity score	(median and range)	30 (0-140)	15 (0-110)*

963